Chapter 5

PROBABILISTIC EARTHQUAKE LOCATION IN 3D AND LAYERED MODELS

Introduction of a Metropolis-Gibbs method and comparison with linear locations

Anthony Lomax and Jean Virieux
Géosciences-Azur, University of Nice - Sophia Antipolis, Valbonne, France

Philippe Volant and Catherine Berge-Thierry
Institut de Protection et de Sûreté Nucléaire, Fontenay-aux-Roses, Paris, France

Key words: 3D models, earthquake location, non-linear optimization, probability function

Abstract: Probabilistic earthquake location with non-linear, global search methods allows the use of 3D models and produces comprehensive uncertainty and resolution information represented by a probability density function over the unknown hypocentral parameters. We describe a probabilistic earthquake location methodology and introduce an efficient Metropolis-Gibbs, non-linear, global sampling algorithm to obtain such locations. Using synthetic travel times generated in a 3D model, we examine the locations and uncertainties given by an exhaustive grid-search and the Metropolis-Gibbs sampler using 3D and layered velocity models, and by a iterative, linear method in the layered model. We also investigate the relation of average station residuals to known static delays in the travel times, and the quality of the recovery of known focal mechanisms. With the 3D model and exact data, the location probability density functions obtained with the Metropolis-Gibbs method are nearly identical to those of the slower but exhaustive grid-search. The location PDFs can be large and irregular outside of a station network even for the case of exact data. With location in the 3D model and static shifts added to the data, there are systematic biases in the event locations. Locations using the layered model show that both linear and global methods give systematic biases in the event locations and that the error volumes do not include the "true" location – absolute event locations and errors are not recovered. The iterative,

C.H. Thurber and N. Rabinowitz (eds.), Advances in Seismic Event Location, 101–134.

linear location method can fail for locations near sharp contrasts in velocity and outside of a network. Metropolis-Gibbs is a practical method to obtain complete, probabilistic locations for large numbers of events and for location in 3D models. It is only about 10 times slower than linearized methods but is stable for cases where linearized methods fail. The exhaustive grid-search method is about 1000 times slower than linearized methods but is useful for location of smaller number of events and to obtain accurate images of location probability density functions that may be highly-irregular.

1. INTRODUCTION

The accurate location of earthquakes and a complete understanding of the location uncertainties are critical to seismotectonic and seismic hazard studies, to "real-time" seismic notification, and to nuclear test ban treaty verification. With the increasing availability of three-dimensional structural models from geologic and geophysical interpretations and seismic travel-time inversion, it is important to have location methods valid for 3D velocity models. Probabilistic earthquake location with non-linear, global-search methods allows the use of 3D models and produces comprehensive uncertainty and resolution information.

A complete, probabilistic earthquake location is represented by a probability density function over the unknown parameters, i.e. three spatial co-ordinates of the hypocenter and an origin time. This hyper-volume representation of a location may include multiple "optimal" solutions and may have a highly irregular form. Many studies of seismicity and seismotectonics make explicit use of a probabilistic representation of earthquake locations (i.e. Wittlinger et al., 1993; Vilardo et al., 1996; Calvert et al., 1997; Gresta et al., 1998; Jones and Stewart, 1997).

Commonly used iterative-linearized location programs produce a single, point solution, the preferred hypocenter, and uncertainty estimates based on Gaussian, or normal, statistics evaluated at this point. Such a solution will be a good representation of the complete, probabilistic location only for the case that the density function has a single optimum and a near-ellipsoidal form. Non-linear, global-search methods can be used to identify irregular volumetric, probability density functions required for complete, probabilistic locations. In addition, unlike linear approaches, these methods can be easily applied with 3D models because they do not require partial derivative information, which is difficult or impossible to obtain in complicated models. However, non-linear, global-search methods can be very time consuming, particularly exhaustive grid-search or pure Monte Carlo methods. For "near real-time" seismic notification and for CTBT

monitoring, it is critical to locate events rapidly, while for seismotectonic and hazard studies, there is often a need to relocate many hundreds or thousands of earthquakes. It is thus of significant practical importance to investigate the performance and completeness of efficient, directed global search methods for probabilistic earthquake location in 3D models.

In this chapter we begin with a discussion of a probabilistic earthquake location and existing location methods. We then discuss the non-linear and linear location methods that we will use, and we introduce an efficient, non-linear, Metropolis-Gibbs, simulated annealing global search method. Using synthetic travel times generated in a 3D model and the ideal case of locating using the same 3D model, we compare the performance of this method for determining complete, probabilistic locations against a less efficient but exhaustive grid-search. We next examine a more useful and realistic case of earthquake location in a layered model using the 3D synthetic travel times. We compare the layered model locations and uncertainties obtained with linear and non-linear methods. For the various location methods in 3D and layered models, we investigate the spatial variation of uncertainties, the relation of average station residuals to know static delays in the travel times, and the quality of the recovery of known focal mechanisms.

2. PROBABILISTIC EARTHQUAKE LOCATION

2.1 Posterior density function (PDF)

The non-linear earthquake location algorithms described in this paper follow the probabilistic formulation of inversion presented in Tarantola and Valette (1982) and Tarantola (1987) and the equivalent methodology for earthquake location (*i.e.* Tarantola and Valette, 1982; Moser, van Eck and Nolet, 1992; Wittlinger, Herquel and Nakache, 1993). This formulation relies on the use of normalized and unnormalized probability density functions to express our knowledge about the values of parameters. Thus, given the normalized density function $f(x)$ for the value of a parameter x, the probability that x has a value between X and $X+\Delta X$ is

$$P(X \le x \le X + \Delta X) = \int_{X}^{X+\Delta X} f(x)dx. \qquad (1)$$

In geophysical inversion we wish to constrain the values of a vector of unknown parameters **p**, given a vector of observed data **d** and a theoretical

relationship $\theta(\mathbf{d},\mathbf{p})$ relating $\mathbf{d}$ and $\mathbf{p}$. When the density functions giving the prior information on the model parameters $\rho_{\mathbf{p}}(\mathbf{p})$ and on the observations $\rho_{\mathbf{d}}(\mathbf{d})$ are independent, and the theoretical relationship can be expressed as a conditional density function $\theta(\mathbf{d}|\mathbf{p})\mu_{\mathbf{p}}(\mathbf{p})$, a complete, probabilistic solution can be expressed as a posterior density function (PDF) $\sigma_{\mathbf{p}}(\mathbf{p})$ (Tarantola and Valette, 1982; Tarantola,1987)

$$\sigma_{\mathbf{p}}(\mathbf{p}) = \rho_{\mathbf{p}}(\mathbf{p}) \int \frac{\rho_{\mathbf{d}}(\mathbf{d})\theta(\mathbf{d}\,|\,\mathbf{p})}{\mu_{\mathbf{d}}(\mathbf{d})} d\mathbf{d} \tag{2}$$

where $\mu_{\mathbf{p}}(\mathbf{p})$ and $\mu_{\mathbf{d}}(\mathbf{d})$ are null information density functions specifying the state of total ignorance.

For the case of earthquake location, the unknown parameters are the hypocentral coordinates $\mathbf{x} = (x, y, z)$ and the origin time T, the observed data is a set of arrival times $\mathbf{t}$, and the theoretical relation gives predicted travel times $\mathbf{h}$. Tarantola and Valette (1982) show that, if the theoretical relationship and the observed arrival times are assumed to have Gaussian uncertainties with covariance matrices $\mathbf{C}_T$ and $\mathbf{C}_t$, respectively, and if the prior information on T is taken as uniform, then it is possible to evaluate analytically the integral over $\mathbf{d}$ in (2) and an integral over origin time T to obtain the marginal PDF for the spatial location, $\sigma(\mathbf{x})$. This marginal PDF reduces to (Tarantola and Valette, 1982; Moser, et al., 1992)

$$\begin{aligned} \sigma(\mathbf{x}) &= K\,\rho(\mathbf{x}) \cdot \exp[-\tfrac{1}{2} g(\mathbf{x})] \\ g(\mathbf{x}) &= [\hat{\mathbf{t}}_0 - \hat{\mathbf{h}}(\mathbf{x})]^T (\mathbf{C}_t + \mathbf{C}_T)^{-1} [\hat{\mathbf{t}}_0 - \hat{\mathbf{h}}(\mathbf{x})]. \end{aligned} \tag{3}$$

In this expression K is a normalization factor, $\rho(\mathbf{x})$ is a density function of prior information on the model parameters, and $g(\mathbf{x})$ is an L2 misfit function. $\mathbf{t}_0$ is the vector of observed arrival times $\mathbf{t}$ minus their weighted mean, $\hat{\mathbf{h}}$ is the vector of theoretical travel times $\mathbf{h}$ minus their weighted mean, where the weights w_i are given by

$$w_i = \sum_j w_{ij}; \quad w_{ij} = [(\mathbf{C}_t + \mathbf{C}_T)^{-1}]_{ij}. \tag{4}$$

Furthermore, Moser et al. (1992) show that the maximum likelihood origin time corresponding to a hypocenter at (x, y, z) is given by

$$T_{ml}(\mathbf{x}) = \frac{\sum_i \sum_j w_{ij}[t_i - h_i(\mathbf{x})]}{\sum_i \sum_j w_{ij}}. \quad (5)$$

The posterior density function (PDF) $\sigma(\mathbf{x})$ given by Equation (3) represents a complete, probabilistic solution to the location problem, including information on uncertainty and resolution. This solution does not require a linearized theory, and the resulting PDF may be irregular and multi-modal because the forward calculation involves a non-linear relationship between hypocenter location and travel-times.

This solution includes location uncertainties due to the spatial relation between the network and the event, measurement uncertainty in the observed arrival times, and errors in the calculation of theoretical travel times. However, realistic estimates of uncertainties in the observed and theoretical times must be available and specified in a Gaussian form through $\mathbf{C}_t$ and $\mathbf{C}_T$, respectively. Absolute location errors due to incorrect velocity structure could be included through $\mathbf{C}_T$ if the resulting travel time errors can be estimated and described with a Gaussian structure. Estimating these travel time errors is difficult and often not attempted. When the model used for location is a poor approximation to the "true" structure (as is often the case with layered model approximations), the absolute location uncertainties can be very large.

2.2 Existing inversion methods and complete, probabilistic locations

In practice, a complete, probabilistic earthquake location is formed by some estimate, throughout the region of significant prior probability $\rho(\mathbf{x})$, of the posterior density function (PDF) $\sigma(\mathbf{x})$ given by Equation (3). Ideally, this solution will include multiple solutions and significant irregularities in the form of the PDF.

2.2.1 Linearized inversion

Direct and iterative linear inversion methods (see Aki and Richards (1980)) can be very rapid for optimization, and have been used frequently in recent years for this reason. These methods can be applied to non-linear problems when the theoretical relationship between the model and the data can be locally approximated by a linear expression and when there is a single, well-defined misfit "basin" containing the optimal solution (i.e., the

problem is not ill-conditioned). If these conditions do not hold, then the results of the inversion, including information on uncertainty and resolution, may be incomplete or unstable, and they will not form a good estimate of the complete, probabilistic solution. In earthquake location, the combined effects of the depth-origin time trade-off, the network-event geometry, reading errors, and gradients or interfaces in the velocity model can result in a highly non-linear and ill-conditioned inverse problem that does not satisfy the above requirements. In this case, the inversion may fail or may produce a solution that is not a good representation of the complete PDF. However, we will see below that for the location of events within a network using a layered velocity model, an iterative linear method such as HYPOELLIPSE (Lahr, 1989) can produce a hypocenter and associated Gaussian uncertainties that are nearly identical to the PDF obtained with global search methods.

2.2.2 Exhaustive global search

Both an exhaustive grid-search and a "crude" Monte-Carlo search (Hammersley and Handscomb, 1967; Keilis-Book and Yanovskaya, 1967; Press, 1968; Wiggins, 1969; Sen and Stoffa, 1995) use global and well-distributed sampling of the model space. Thus the results obtained with these search methods can be used to estimate the PDF $\sigma(\mathbf{x})$ and hence to obtain complete, probabilistic locations. However, both methods are inefficient for problems with many unknown parameters, large parameter spaces, or time consuming forward calculations, because the number of models that must be tested can be very large. These methods have been successfully applied to earthquake hypocenter determination (Sambridge and Kennett, 1986; Kennett, 1992; Shearer, 1997; Dreger et al. 1998), and to probabilistic location (Moser, van Eck and Nolet, 1992; Wittlinger, Herquel and Nakache, 1993; Calvert et al., 1997), but their inefficiency may impose unacceptable limitations on the number of events or the size of the search volume.

Below we will use a nested grid-search as one of our non-linear, global location methods. This method gives excellent recovery of the location PDF $\sigma(\mathbf{x})$, but requires considerable calculation time and computing resources.

2.2.3 Directed, stochastic search

Directed, stochastic search techniques (Sen and Stoffa, 1995) include evolutionary, adaptive, global search methods such as the genetic algorithm (Goldberg, 1989; Holland, 1992; Stoffa and Sen, 1991; Sambridge and Drijkoningen, 1992) and simulated annealing (Kirkpatrick et al., 1983; Rothman, 1985; Tarantola, 1987). Most of these methods were developed

for *optimization*, the identification of *some* very good solutions, which is equivalent to identifying global or local maxima of a solution PDF $\sigma(\mathbf{x})$. But in general these methods do not use a well-distributed sampling of the model space that can produce complete, probabilistic solutions to inverse problems. For example, the genetic algorithm obtains samples that cluster in small regions near locally optimum solutions and consequently cannot be used to obtain the global structure of a PDF (e.g. Goldberg and Richardson, 1987; Stoffa and Sen, 1991; Nolte and Frazer, 1994; Lomax and Snieder, 1995). Similarly, with simulated annealing, the interaction of the variable "temperature" parameter and step size with the local structure of the target function can lead to a slow gain of information about the global structure of this function (Scales et al., 1992). In practice, this leads to convergence and stalling near a locally optimum solution and a poorly distributed sample distribution.

Though not directly applicable to complete, probabilistic location, the genetic algorithm and simulated annealing are excellent for non-linear, earthquake hypocenter determination because of their efficiency (Sambridge and Gallagher, 1993; Billings, 1994).

2.2.4 Importance sampling – the Metropolis-Gibbs algorithm

The efficiency of a Monte Carlo algorithm used to estimate properties of a target function can be increased by choosing a sampling density which follows the function as closely as possible (Hammersley and Handscomb, 1967; Lepage, 1978; Press et al., 1992). Techniques that follow this rule are referred to as *importance sampling* methods, these were originally developed in physics for fast and accurate numerical integration of multi-dimensional functions.

The target function is unknown, however, and consequently the optimum importance sampling distribution cannot be determined a priori. But the efficiency can still be improved by adjusting (or adapting or evolving) the sampling by incorporating information gained from previous samples so that the sampling density tends towards the target function (Lepage, 1978; Press et al., 1992; Mosegaard and Tarantola, 1995; Sen and Stoffa, 1995). For example, importance sampling to determine the earthquake location PDF, Equation (3), can be obtained by beginning with a sampling that follows the prior density function $\rho(\mathbf{x})$ and then adjusting the sampling as the search progresses so that the sampling density approaches the location PDF $\sigma(\mathbf{x})$.

An importance sampling technique that is relevant to inversion for complete, probabilistic solutions is the Metropolis-Gibbs version of simulated annealing. The Metropolis-Gibbs sampling procedure is based on an algorithm (Metropolis et al., 1953) for the simulation of the distribution

of atoms in a gas at a given temperature. Other importance sampling methods are discussed in Hammersley and Handscomb (1967), Lepage (1978) and in Press et al. (1992) in the context of numerical integration.

The Metropolis-Gibbs sampler (Sen and Stoffa, 1995; Mosegaard and Tarantola, 1995) is similar to simulated annealing with a constant temperature parameter. In the context of our earthquake location problem, the Metropolis-Gibbs algorithm performs a random walk in the solution space (x, y, z) with nearby trial moves which are accepted or rejected according to the PDF $\sigma(\mathbf{x})$ (after evaluation of the forward problem). Mosegaard and Tarantola (1995) show that this algorithm generates a set of "accepted" samples that are distributed according to the PDF $\sigma(\mathbf{x})$; it is therefore an importance sampling method. They also show that, in the limit of a very large number of trials, it will not become permanently "trapped" near a locally optimum solution and consequently can produce global sampling.

Because it is a random walk technique, the Metropolis-Gibbs sampler may perform well even if the volume of the significant regions of $\sigma(\mathbf{x})$ is small relative to the volume of the prior search space $\rho(\mathbf{x})$; this is usually the case in earthquake location. However, because it must use small steps in the model space between consecutive samples, and in practice the number of samples is limited, it may be subject to stalling near strong locally optimal solutions if $\sigma(\mathbf{x})$ is a complicated function. In addition, since samples are accepted or rejected *after* evaluation of the forward problem, the number of evaluations of the forward theory may be much larger that the set of "accepted" samples obtained.

Below we will introduce a new Metropolis-Gibbs algorithm for probabilistic earthquake location. We will show that it is much more computationally efficient than a grid search while producing nearly identical definition of the complete location PDF $\sigma(\mathbf{x})$ when this function is not highly irregular.

3. NON-LINEAR, PROBABILISTIC LOCATIONS IN 3D: NONLINLOC

For the non-linear, global search locations in this chapter, we use a set of location programs called NonLinLoc. This software can be obtained over the internet at the ORFEUS Seismological Software Library (http://orfeus.knmi.nl) under the "software links" page. The location program in NonLinLoc can be used with 3D velocity models; it produces an estimate of the posterior density function (PDF) for the spatial hypocenter location, $\sigma(\mathbf{x})$, using either a systematic grid-search or a stochastic,

Metropolis-Gibbs sampling approach. The location algorithm follows the probabilistic inversion approach of Tarantola and Valette (1982), described above, and the earthquake location methods of Tarantola and Valette (1982), Moser et al. (1992) and Wittlinger et al. (1993).

A grid of PDF values obtained by grid-search, samples drawn from this grid, or samples of the PDF obtained by the Metropolis-Gibbs sampler, represent the complete, probabilistic, spatial solution to the earthquake location problem. This solution indicates the uncertainty in the spatial location due to Gaussian-distributed picking and travel-time calculation errors, the network-event geometry, and the incompatibility of the picks. The location uncertainty will in general be non-ellipsoidal (non-Gaussian) because the forward calculation involves a non-linear relationship between hypocenter location and travel-times.

To make the location program efficient for complicated 3D models, the travel-times between each station and all nodes of an *x,y,z* spatial grid are calculated once using a 3D version (Le Meur, 1994; Le Meur, Virieux and Podvin, 1997) of the eikonal finite-difference scheme of Podvin and Lecomte (1991) and then stored on disk as travel-time grid files. This storage technique has been used by Wittlinger et al. (1993), and in related approaches by Nelson and Vidale (1990) and Shearer (1997). The forward calculation during location reduces to retrieving the travel-times from the grid files and forming the misfit function $g(\mathbf{x})$ in, Equation (3).

3.1 Travel-time and take-off angles calculations

The travel times between a station and all nodes of a 3D grid are calculated using the eikonal finite-difference scheme of Podvin and Lecomte (1991). This algorithm and related methods (Vidale, 1988) use a finite-differences approximation of Huygen's principle to find the first arriving, infinite frequency travel times at all nodes of the grid. The algorithm of Podvin and Lecomte (1991) gives stable recovery of diffracted waves near surfaces of strong velocity contrast and thus it accurately produces travel times for diffracted and head waves. A limitation of the current 3D version of the method is a restriction to cubic grids. This may lead to excessively large travel-time grids if a relatively fine cell spacing is required along one dimension since the same spacing must be used for the other dimensions. This can be a problem for regional studies where a fine node spacing in depth is necessary, but the horizontal extent of the study volume can be much greater than the depth extent. Thus a modification of the travel times calculation to allow use of an irregular grid would be very useful.

After the travel times are calculated throughout the grid, the NonLinLoc program uses the gradients of travel-time at the node to estimate the take-off

angles at each node. Two gradients are estimated for each axis direction x, y, and z, one G_{low} between the node and its preceding neighbour along the axis, and a second G_{high} between the following neighbour and the node. The total gradient G_{axis} along an axis is the mean of these two gradients; the total gradient along the three axes determines the vector gradient of travel-time. The direction opposite to the vector gradient of travel-time gives the ray take-off angles for dip and azimuth. An estimate of the quality of the angle determination is given by a comparison of the magnitudes and signs of G_{low} and G_{high}. If these two values are not similar, then there may be two rays which arrive nearly simultaneously at the station, and the take-off angle determination at the node may be unstable.

3.2 Grid-Search Algorithm

The grid-search algorithm in NonLinLoc performs successively finer, nested grid searches within a spatial x,y,z volume to obtain an estimate of the location PDF, Equation (3). The grid-search performs a systematic, exhaustive coverage of the search region and thus can identify multiple optimal solutions and highly irregular confidence volumes. However, the grid-search is very time consuming relative to the Metropolis-Gibbs sampler and linear location techniques. It also requires a careful selection of the grid sizes and node spacing, otherwise, relative to the size of the most significant region of the PDF, the fine search grids may be too large (giving low resolution) or too small (leading to truncation of the PDF).

3.2.1 Procedure

An initial grid with a fixed size, number of nodes, and location defines the full search region. Subsequent, nested grids are centred automatically on the optimal hypocentral node of the containing grid in one or more of the x,y,z directions. The nested grids are typically smaller in size, but may have more nodes than the containing grid.

For every node of each location grid, the grid-search algorithm must obtain travel-times for every observation from the corresponding travel-time grid files. For 3D structures these files may be very large, and with many observations there will be many such files. To read these files efficiently without storing them entirely in memory, the search is performed systematically throughout each location grid with the x index varying last. Thus, it is only necessary to read into memory a 2D y-z plane or "sheet" corresponding to the current x index for each observation.

With these travel times, Equation (3) is evaluated to obtain a non-normalized location PDF value, which is stored at the appropriate node in

the search grid in memory. When the grid-search for the final fine grid is complete, the gridded PDF values are normalized by assuming that the integral of the PDF over the search volume is unity. A set of samples of the PDF can be drawn from this normalized grid. The normalized fine grid, the PDF samples, and additional location results (see below) are saved to disk files.

3.3 Metropolis-Gibbs Sampling Algorithm

The Metropolis-Gibbs sampler introduced here performs a directed random walk within a spatial *x,y,z* volume to obtain a set of samples that follow the location PDF. This algorithm is similar to those described in Sen and Stoffa (1995) and Mosegaard and Tarantola (1995), with the addition of three distinct sampling stages to obtain adaptively an optimal step size for the walk.

Like the grid-search, the Metropolis-Gibbs sampler does not require partial derivatives and thus can be used with complicated 3D velocity structures. This method performs well with moderately irregular (non-ellipsoidal) PDFs with a single optimum solution, but because it is a stochastic search it may give inconsistent recovery of very irregular PDFs with multiple optimal solutions. The Metropolis-Gibbs sampler is only moderately slower (about 10 times) than linearized, iterative location techniques, and is much faster (about 100 times) than the grid-search. Because the Metropolis-Gibbs method samples the search space stochastically, it runs fastest with the full 3D travel-time grid files in memory. If memory limitations, the number of observations, or the size of the 3D travel-time grids prevents this, then the travel-time grids must be accessed on disk, and the search may run very slowly.

3.3.1 Procedure

The Metropolis-Gibbs sampler used in the program NonLinLoc for earthquake location consists of a directed walk in the solution space (x, y, z) which tends towards regions of high likelihood for the location PDF, $\sigma(\mathbf{x})$, given by Equation (3). At each step, the current walk location $\mathbf{x}_{curr}$ is perturbed by a vector $d\mathbf{x}$ of arbitrary direction and given length l to give a new location $\mathbf{x}_{new}$. The likelihood $\sigma(\mathbf{x}_{new})$ is calculated for the new location and compared to the likelihood $\sigma(\mathbf{x}_{curr})$ at the current location. If $\sigma(\mathbf{x}_{new}) \geq \sigma(\mathbf{x}_{curr})$, then the new location is accepted. If $\sigma(\mathbf{x}_{new}) < \sigma(\mathbf{x}_{curr})$, then the new location is accepted with probability $P = \sigma(\mathbf{x}_{new}) / \sigma(\mathbf{x}_{curr})$. When a new location is accepted it becomes the current location and may be saved as a sample of the location PDF.

In earthquake location, the dimensions of the significant regions of the location PDF can vary enormously and are not known a priori. It is important to choose an initial step size large enough to allow global exploration of the search volume, and to obtain a final step size that gives good coverage of the location PDF while resolving details and irregular structure of the PDF. The NonLinLoc Metropolis-Gibbs sampler uses three distinct sampling stages to determine adaptively an optimal step size l for the walk:

1. A *learning* stage where the step size is fixed and relatively large. The walk can explore globally the search volume and migrate towards regions of high likelihood. "Accepted" samples are not saved.
2. An *equilibration* stage where the step size l is adjusted in proportion to the standard deviations (s_x, s_y, s_z) of the spatial distribution of all previously "accepted" samples obtained after the middle of the learning stage. After each new accepted sample, the standard deviations are updated and the step size l is set equal to $f_s\,(s_x s_y s_z / N_s)^{1/3}$, where N_s is the total number of samples to be accepted during the saving stage, and f_s=8 is a step size scaling factor. This formula sets l in proportion to the cell size required to tile with N_s cells the rectangular volume with sides s_x, s_y and s_z. The walk can continue to migrate towards or may begin to explore regions of high likelihood. "Accepted" samples are not saved.
3. A *saving* stage where the step size l is fixed at its final value from the equilibration stage. The walk can continue to explore regions of high likelihood. "Accepted" samples are assumed to follow the location PDF and can be saved, but there may be a waiting time of several samples between saves to insure the independence of saved samples.

The NonLinLoc Metropolis-Gibbs sampling algorithm is initialized as follows:

1. The walk location is set at the x,y position of the station with the earliest arrival time and non-zero weight, at the mean depth of the search region.
2. If the initial step l size is not specified, it is set to the cell size required to tile with N_s cells the plane formed by the two longest sides of the initial search region. N_s is the total number of samples to be accepted during the saving stage, including samples that are skipped between saves.

The rejection by the algorithm of new walk locations for a large number of consecutive tries (the order of 1000 tries) may indicate that the last "accepted" sample falls on a sharp likelihood maxima that is narrower than the current step size. To allow the search to continue in this case, the new location is accepted unconditionally and the step size is reduced by a factor of two.

In the case that the size of the location PDF is very small relative to the search region, the algorithm may fail to locate the region of high likelihood or obtain an optimal step size. In this case the size of the search region must be reduced or the size of the initial step size adjusted. A more robust solution to this problem may be to add a temperature parameter to the likelihood function, as with simulated annealing. This variable parameter could be set to increase the effective size of the PDF during the learning and equilibration stages so that the region of high likelihood is located efficiently, and then set to 1 during the saving stage so that the true PDF is imaged.

3.4 Additional location results

In addition to an estimate of the location PDF, the NonLinLoc program determines an optimal hypocenter, traditional Gaussian statistics and other location parameters.

3.4.1 Maximum likelihood hypocenter

The maximum likelihood (or minimum misfit) point of the complete, non-linear location PDF is selected as an "optimal" hypocenter. The significance and uncertainty of this maximum likelihood hypocenter cannot be assessed independently of the complete solution PDF. The maximum likelihood hypocenter location is used for the determination of ray take-off angles, for the determination of phase residuals, and for magnitude calculation. The ray take-off angles can be used for a first-motion fault plane determination.

3.4.2 Gaussian estimators

"Traditional" Gaussian or normal estimators, such as the expectation $E(\mathbf{x})$ and covariance matrix $\mathbf{C}$ may be obtained from the gridded values of the normalized location PDF or from samples of this function (e.g. Tarantola and Valette, 1982; Sen and Stoffa, 1995). For the grid case with nodes at $\mathbf{x}_{i,j,k}$,

$$E(\mathbf{x}) = \Delta V \sum_{i,j,k} \mathbf{x}_{i,j,k} \sigma(\mathbf{x}_{i,j,k}), \tag{6}$$

where ΔV is the volume of a grid cell. For N samples drawn from the PDF with locations $\mathbf{x}_n$,

$$E(\mathbf{x}) = \frac{1}{N}\sum_{n} \mathbf{x}_n , \tag{7}$$

where the PDF values $\sigma(\mathbf{x}_n)$ are not required since the samples are assumed distributed according to the PDF. For both cases, the covariance matrix is then given by

$$\mathbf{C} = E[(\mathbf{x} - E(\mathbf{x}))\cdot(\mathbf{x} - E(\mathbf{x}))^T]. \tag{8}$$

The 68% confidence ellipsoid can be obtained from singular value decomposition (SVD) of the covariance matrix **C**, following Press *et al.* (1993; their sec. 15.6 and Equations 2.6.1 and 15.6.10). The SVD gives

$$\mathbf{C} = \mathbf{U}[diag\, w_i]\mathbf{V}^{\mathrm{T}}, \tag{9}$$

where **U** and **V** are square, symmetric matrices and w_i are singular values. The columns $\mathbf{V}_i$ of **V** give the principle axes of the confidence ellipsoid. The corresponding semi-diameters for a 68% confidence ellipsoid are $(3.53 w_i)^{1/2}$, where 3.53 is the $\Delta\chi^2$ value for 68.3% confidence and 3 degrees of freedom. The Gaussian estimators and resulting confidence ellipsoid will be good indicators of the uncertainties in the location only in the case where the complete, non-linear PDF has a single maximum and has an ellipsoidal form.

4. LINEAR LOCATIONS: HYPOELLIPSE

The HYPOELLIPSE program (Lahr, 1989) performs local and near regional earthquake locations in layered or gradient-layered 1D models. The program uses Geiger's method (Geiger, 1912) to find a hypocenter that minimizes the root-man-square misfit between observed and calculated travel times by iterative update of trial locations. The updates are obtained from a damped least-squares inversion of the matrix of partial derivatives of travel time with respect to the three spatial hypocenter coordinates at the current trial location. Because the location problem is non-linear, this matrix represents a "linearization" of the problem, and the final solution must be obtained though iteration. Gaussian uncertainty information for the final hypocenter is given in the form of a 68% spatial confidence ellipsoid obtained from analysis of the matrix of partial derivatives at this solution. This ellipsoid forms a local approximation to the complete PDF for the location.

There are many programs to perform linear, iterative earthquake location following Geiger's method. We choose HYPOELLIPSE for this study because the 68% confidence ellipsoid can be compared directly to the complete PDF for the location obtained with the non-linear methods.

HYPOELLIPSE has options to perform a grid search in depth and to change individual observation weights during iteration based on residuals, distance or azimuth to hypocenter, and other quantities. For simplicity and compatibility we do not use these options in this study, but note that they may have significant effects on the hypocenter and confidence ellipsoid determinations, particularly for poorly constrained events.

5. A STUDY OF SYNTHETIC LOCATIONS

We examine various earthquake location scenarios using synthetic travel times for a 3D model. The purpose of this study is to 1) validate and compare the performance of the efficient Metropolis-Gibbs sampler algorithm against the slow but exhaustive grid-search, 2) examine the ideal case of location using the "correct" 3D velocity model, 3) study the realistic case of location in an "incorrect" layered model, and 4) compare the locations and uncertainties obtained by the linear, local method with those of the non-linear, global-search methods. Other synthetic location studies which address some of these issues have been performed by Pavlis (1986) and by Schwartz and Nelson (1991).

5.1 The synthetic problem

The station geometry, velocity structure and event locations are based on characteristics of the Institut de Protection et de Sûreté Nucléaire (IPSN) Durance micro-earthquake network and study region in southern France (Mohammadioun and Dervin, 1995; Volant et al., 2000). We select 11 IPSN stations to obtain a network of about 60 km by 30 km and typical station spacing of 10 to 20 km. For plotting we use a rotated, left-handed rectangular coordinate system where the Y axis is oriented along the true geographic azimuth N30°E, and Z is positive downwards.

The 3D velocity structure (Figure 1) is a simplified, 2.5D version of a preliminary 3D model for the Durance region. To reflect the transpressive tectonics of the region we include a strong velocity contrast of about 20% across a vertical plane through the network at Y=0 (representing the Middle-Durance fault) and a contrasts of 6 to 12% across a dipping plane that intersects this "fault" at depth. The S velocities are determined from the P velocity model using a V_P/V_S ratio of 1.75.

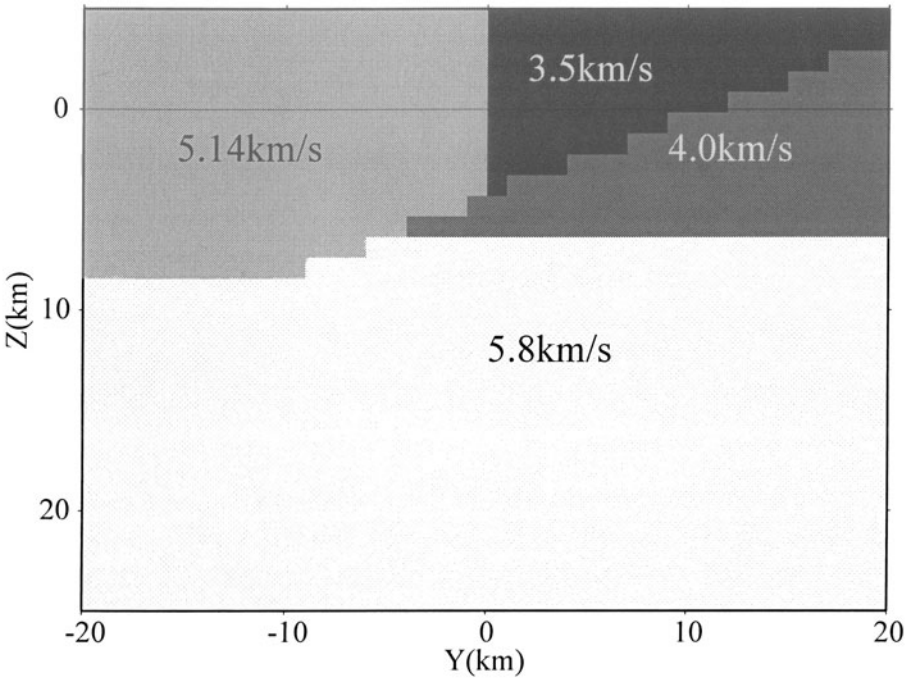

Figure 1. 3D velocity structure used for generating synthetic arrival times and for 3D model locations. The P velocity structure is shown in Y-Z cross section; the model is invariant in the X direction. S velocities are determined from the P velocity model using a V_P/V_S ratio of 1.75.

We consider 27 synthetic "events" regularly spaced on a vertical plane which is coincident with the "fault" plane (Y=0) and which passes through the network (Figure 2). The events are located up to 20 km outside of the network and between 0 and 20 km in depth.

The basic data set for the synthetic locations consists of 15 simulated P or S arrival times at the network stations for each of the 27 events. The times are calculated using the 3D velocity structure and the same eikonal finite-difference algorithm (Podvin and Lecomte, 1991) used for the NonLinLoc event locations. We generate a set of exact, "noise free" arrival times, and a set of arrival times with station "statics" by adding constant shifts to the times at each station of ±0.1 or ±0.2 second for P and S arrivals, respectively (Table 1). For an individual event, these statics can be considered as picking errors or as general velocity model errors; for the 27 events together these statics should be considered as errors in the velocity model near each station.

For both sets of arrival times and for all location methods the reading errors are set equal to the magnitude of the corresponding static shift (Table 1). The squares of the reading errors will form the diagonal terms of the

diagonal covariance matrix $\mathbf{C}_t$ for the observed arrival times. For compatibility with HYPOELLIPSE, the covariance matrix $\mathbf{C}_T$ for theoretical relationship is set to the zero matrix $\mathbf{0}$; in practice the terms of this matrix should reflect the uncertainty in the theoretical travel times due to errors in the velocity model. We also generate synthetic first-motions for each P arrival corresponding to a pure left-lateral mechanism (strike=90°, dip=90°, rake=180°) in the unrotated, geographic coordinate frame.

Table 1. Station static shifts and reading errors

Station	phase	static shift (sec)	reading error (sec)
ART1	P	0.1	0.1
BLV1	P	-0.1	0.1
BST	P	0.1	0.1
BST	S	0.2	0.2
CAD	P	-0.1	0.1
CAD	S	-0.2	0.2
ESC	P	0.1	0.1
ESC	S	0.2	0.2
GRX	P	-0.1	0.1
JOU	P	0.1	0.1
JOU	S	-0.2	0.2
MEY	P	0.1	0.1
REV1	P	-0.1	0.1
OBS1	P	0.1	0.1
VAL1	P	-0.1	0.1

For the 1D model locations we use a two-layer over half-space velocity model (Table 2) where the layer depth differs from that of any horizontal interface in the 3D model, and with a different V_P/V_S ratio than the 3D model. The 1D model is constructed arbitrarily and not by averaging or transformation of the 3D model, nor by any analysis of the simulated arrival times. Thus the 1D model is not an optimized model for the problem, but represents a typical, "incorrect" reference model as might be used in a preliminary seismicity study for a region.

Table 2. 1D, layered velocity model (V_P/V_S = 1.85)

Depth to top (km)	P velocity (km/sec)	S velocity (km/sec)
-	4.5	2.43
4.5	5.8	3.14
30	8.0	4.32

Each grid-search location is run with an initial grid size of 100 by 100 km horizontally centred at X=0, Y=0 and a depth range of –5 to 30 km, with a node spacing of 2 km horizontally and 1 km vertically. Two further nested grids are each centred on the optimal hypocentral node of the preceding grid.

The final grid has a size of 10 by 10 km horizontally and 15 km in depth with a node spacing of 0.1 km, giving 1.5 million nodes. A total of about 1.7 million evaluations of the forward problem are performed.

Each Metropolis-Gibbs location is run with 1000 "accepted" samples in the learning stage, 4000 in the equilibration stage, and 5000 in the saving stage. This gives a total of 10000 "accepted" samples, which typically requires the testing (evaluation of the forward problem) at about 14000 locations. During the saving stage every fifth "accepted" sample is kept to give a total of 1000 samples of the PDF.

The HYPOELLIPSE locations use the same arrival times, arrival time uncertainties and layered model as the non-linear locations. HYPOELLIPSE is run for a maximum of 50 iterations, without any re-weighting of the observations during the iterations.

The relative calculation times for the 27 event locations for the three methods are HYPOELLIPSE 1 unit, Metropolis-Gibbs 10 units, and grid-search 1000 units, where a unit is the order of several second on a desktop workstation.

In the following we use the notation $[x,z]$ to identify events using their approximate coordinates on the (X-Z) sections.

5.2 Location with 3D models

5.2.1 Exact data: verification of the algorithms and uncertainties due to station-event geometry

We first perform grid-search and Metropolis-Gibbs locations using the exact synthetic travel times and the correct 3D model. The location results are shown in Figure 2.

The Metropolis-Gibbs and grid-search PDFs and Gaussian estimators are very similar and the maximum likelihood hypocenters from both methods give excellent recovery of the true locations and origin times. Typical location errors for the grid-search are ~0km horizontally, <0.05km in depth and <0.01sec in origin time. For Metropolis-Gibbs the horizontal errors are <0.1km outside the network and <0.02km inside, <0.1km in depth (except for 2 events outside the network with errors of 0.25 and 0.15km) and < 0.01 in origin time. There is a very good agreement between the grid-search PDFs, which we take as near exact, and those for the Metropolis-Gibbs sampler (Figure 2). However, the Metropolis-Gibbs method does not recover the detailed form of the most irregular PDFs (i.e. events [–40,6] and [40,6]).

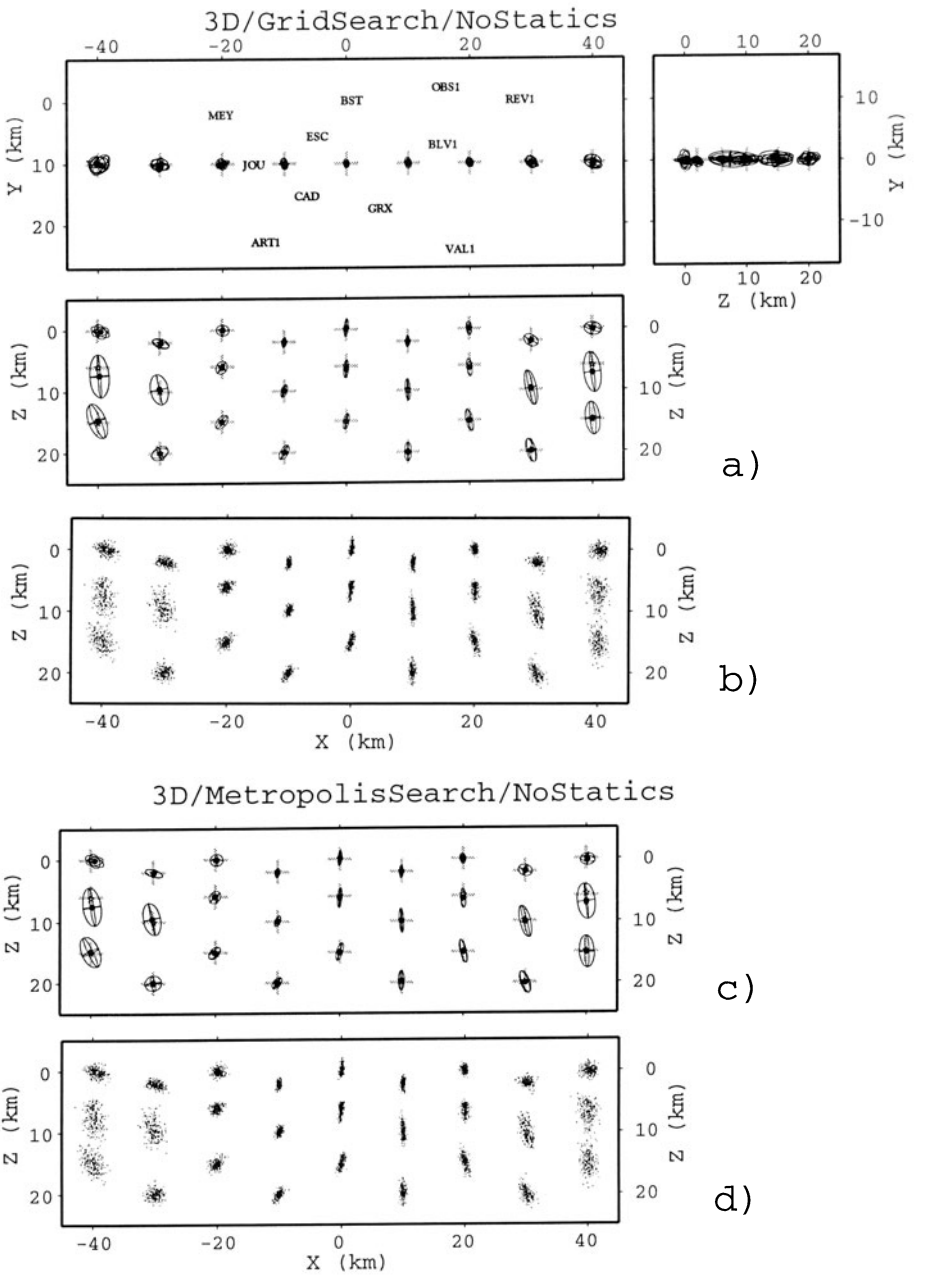

Figure 2. Location with 3D model and exact data. a) Grid-search locations in map view (XY) and perpendicular (ZY) and parallel (XZ) to the event plane. b) Grid-search PDF density plots in XZ section. c) Metropolis-Gibbs locations in XZ section. d) Metropolis-Gibbs PDF density plots in XZ section. Crosses: true event locations; stars: maximum likelihood hypocenters, dots: expectation hypocenters, ellipses: projections of 68% confidence ellipsoids.

For this "noise free" simulation with the correct velocity model, the shapes and sizes of the PDFs reflect the assumed reading errors, variations of the velocity model within the PDF, and the geometric relation between the events and stations (through the distribution of ray take-off angles). The location uncertainties are smallest and generally ellipsoidal within the network; they increase in size outside of the network, where some (i.e., events [–40,6] and [40,6]) become irregularly shaped and have off-center expectation hypocenter locations. The uncertainties are generally largest in depth, typically 2-4 times the horizontal uncertainty, even within the network. The depth uncertainty is smallest for the events within the network and with the least epicentral distance to the nearest station (e.g., events under station JOU). All of these variations reflect the improved distribution of ray take-off angles for events within the network and at shallower depths.

The effect of the horizontal interface in the velocity model at 5km depth is seen in the truncation of the tops of several PDFs (i.e., events [–20,6], [0,6] and [20,6]), and in a sharp bend in the PDFs for events [-40,6] and [40,6].

5.2.2 Data with station "statics": an ideal location scenario

We next examine Metropolis-Gibbs locations in the correct 3D model using the synthetic travel times with station statics. These results represent an ideal but realistic scenario where an accurate larger scale velocity model is available (perhaps determined independently by active source refraction experiments), but where there remain errors in the model near the stations. The locations obtained with the Metropolis-Gibbs sampler are shown in Figure 3. As above, these results are almost identical to those for the grid-search (not shown).

The maximum likelihood and expectation hypocenters in Figure 3 are shifted up to 5 km in depth and 2 km horizontally from the "true" event locations. In plan view (XY), the locations bend away from the plane of "true" locations with a larger shift for events outside of the network; in depth section (ZY), the distance of the locations from the plane of "true" locations increases in with increasing depth. Thus the added station statics do not cancel each other and are systematically biasing the locations.

In general, the size and orientation of the location uncertainties are similar to those from the previous simulation with exact data. One exception is the distorted and tilted PDF and confidence ellipsoid for the event near [40,5]. The station static errors have caused a shift in the PDF for this event such that it interacts more strongly with the model interface at 5 km depth. Another exception is the more elongated PDF and confidence ellipsoid for the event near [40,11]. Many of the confidence ellipsoids and PDF scatter

samples do not contain the "true" location, even though the assigned reading errors (Table 1) are of the same magnitude as the static shifts. This result probably reflects a bias in the locations caused by the application of static shifts at a small number of irregularly distributed stations.

This example illustrates that formal location uncertainties are insensitive to the station static shifts and do not reflect the absolute location errors. Apparently the uncertainties depend primarily on the station geometry and assumed observational errors. Station statics or, equivalently, small errors in the model near the stations, lead mainly to a bias in the location.

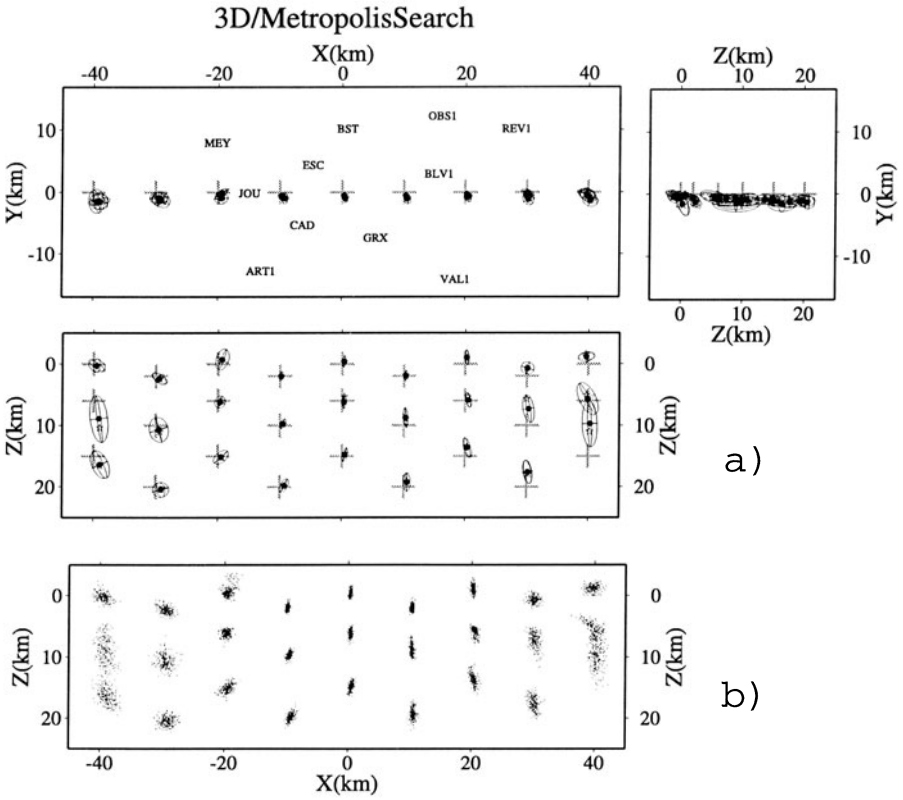

Figure 3. Location with 3D models and station static shifts. a) Metropolis-Gibbs locations in map view (XY), and views perpendicular (ZY) and parallel (XZ) to the event plane. b) Metropolis-Gibbs PDF density plots in XZ section. Crosses: true event locations; stars: maximum likelihood hypocenters, dots: expectation hypocenters, ellipses: projections of 68% confidence ellipsoids.

5.3 Location with layered models

We next perform grid-search, Metropolis-Gibbs, and linearized HYPOELLIPSE locations in the 1D layered model (Table 2) using the 3D model synthetic travel times with station statics. With this realistic and typical location scenario, we examine the location uncertainties and biases due to the use of a model that differs significantly from the true earth structure. We also compare the ellipsoidal approximations to the location PDFs given by HYPOELLIPSE to the complete PDFs and associated ellipsoids obtained with the non-linear, global search location algorithms.

5.3.1 Metropolis-Gibbs sampler

The maximum likelihood and expectation hypocenters and the PDF samples for the Metropolis-Gibbs location in the 1D model are shown in Figure 4. In depth section (ZY) the 1D model locations group near a vertical plane which is shifted significantly from the plane of "true" locations (the plane Y=0). In plan view (XY) the locations bend away from the plane of "true" locations with a shift of about 4 km horizontally towards higher velocity side of the 3D model for locations within network, increasing to about 10 km for events outside of the network. The (XZ) section shows that, relative to the "true" locations, most of the 1D locations are "pulled" towards the network centre and the relative locations are not preserved. There is a larger shift for deeper events and for events outside the network which are shifted up to 10 km shallower in depth and up to 8 km horizontally. The shifts in the (XZ) section are consistent with the generally lower velocities in the 1D layered model relative to the 3D model.

Overall, the location PDFs and confidence ellipsoids have the same or smaller size and a similar orientation to those for the 3D model. Two exceptions are the events near [–35,5] and [35,5] which have enlarged, elongated and bent PDFs and a maximum likelihood hypocenter located much shallower than the expectation hypocenter. The apparent decrease in uncertainty for some locations may be related to the shallower depth of the 1D locations and to the lower velocities in the 1D models. As with the 3D locations with station statics, the confidence ellipsoids and PDF samples do not contain the "true" locations and thus do not reflect the absolute location errors.

5.3.2 Grid search

Most of the grid-search locations and uncertainties are very similar to those obtained with Metropolis-Gibbs (Figure 4). Two exceptions are the

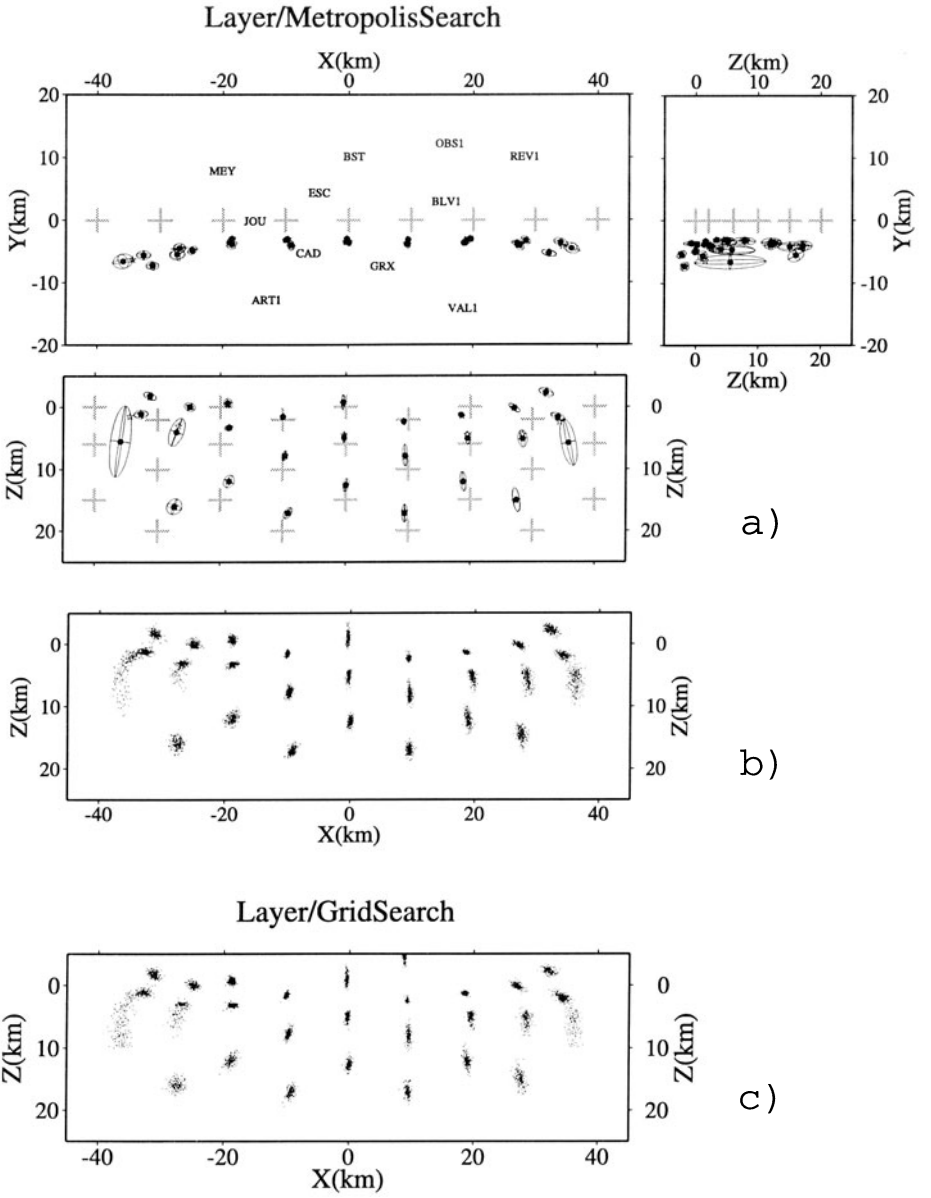

Figure 4. Location with the layered model. a) Metropolis-Gibbs locations and 68% confidence ellipsoids in map view (XY) and perpendicular (ZY) and parallel (XZ) to the event plane. b) Metropolis-Gibbs PDF density plots in XZ section. c) Grid-search PDF density plots in XZ section. Crosses: true event locations; stars: maximum likelihood hypocenters, dots: expectation hypocenters, ellipses: projections of 68% confidence ellipsoids.

events at [-37,5] and [36,7] where the fine grid-search volume is not large enough to contain the elongated PDF which is clipped at depth. This problem can be avoided by extending the fine grid in depth, at the expense of increased calculation time. Other exceptions are the events at [-27,4], [36,7] and [10,2] where the Metropolis-Gibbs PDFs differ notably from those of the grid-search. Apparently for these events the PDF is of sufficient complexity that it cannot be fully recovered by the Metropolis-Gibbs sampler. This is most clear for the event at [10,2] where the grid-search PDF shows two completely separate maxima in the PDF, one at a depth of about 2 km and one at the top of the search region at –5 km. The Metropolis-Gibbs sampler recovers only the deeper of these two solutions.

5.3.3 HYPOELLIPSE

The HYPOELLIPSE hypocenters and confidence ellipsoids for locations in the layered model are shown in Figure 5. For events within the network (-20km $\leq$ X $\leq$ 20km) most of the HYPOELLIPSE hypocenters and confidence ellipsoids are nearly identical to the corresponding Metropolis-Gibbs and grid-search results (Figure 4). Though, like the Metropolis-Gibbs sampler, HYPOELLIPSE only recovers the deeper of the two solutions for the event at [10,2]. Two other exceptions are the events at [0,5] and at [20,5] both of which have a much larger depth uncertainty with HYPOELLIPSE than Metropolis-Gibbs. This discrepancy can be explained for both events by examining the form of the grid-search PDF for the event near [20,5] (Figure 6). The PDF is strongly distorted at the model layer boundary at 4.5km depth and the maximum likelihood hypocenter is located on this boundary. At this boundary the gradients in the misfit function (i.e., $g(\mathbf{x})$ in Equation (3)) will be discontinuous which can lead to convergence problems for a linear method like HYPOELLIPSE. For this event, HYPOELLIPSE converges to a hypocenter just below the boundary. In this region the misfit function and PDF change very slowly with depth (Figure 6) because the first arriving rays from points just below the boundary are "head waves" with horizontal take-off directions. Thus, for the linear approach, the partial derivatives of travel-time with respect to depth will be near zero in this region, and the corresponding error estimates very large, leading to the elongated Z axis of the confidence ellipsoid. Note that for these 2 events the difference in expectation and maximum likelihood hypocenters obtained by the global search methods is an indicator of complexity in the PDFs.

For events outside of the network, there are significant differences between the HYPOELLIPSE and non-linear, global search locations. For many events with highly irregular PDFs, the HYPOELLIPSE error ellipsoids are greatly elongated in the Z direction, indicating poor depth constraint, and

the HYPOELLIPSE hypocenters are far from the maximum likelihood point of the PDFs. Such events include [-35,5], [28,5], [36,7], and [39,6], which correspond to true event locations [-40,6], [30,10], [40,15], and [40,0], respectively. Because of the presence of the layer boundary at 4.5km, and their location outside the network, the PDFs for these events are highly irregular (Figure 4). For the event with true location [40,0], it is important to note that the global optimum solution, as indicated by the grid-search or Metropolis-Gibbs maximum likelihood point, is located near [32,-2], more than 10km from the HYPOELLIPSE hypocenter near [39,6].

A comparison with the un-clipped grid-search PDF for the event near [36,7] is shown in Figure 6. The HYPOELLIPSE hypocenter is located near a secondary maximum of the grid-search PDF, probably because the global maximum is in a basin with a much smaller volume than that of the secondary maximum and because the starting depth of 10km used for HYPOELLIPSE is closer to the secondary maximum. The hypocenter is in a relatively flat region of the PDF, which explains the large size of the confidence ellipsoid in the depth direction since uncertainty is inversely proportional to the second derivative of the misfit surface. The very small gradients of the PDF in the Z direction near the hypocenter make the linear

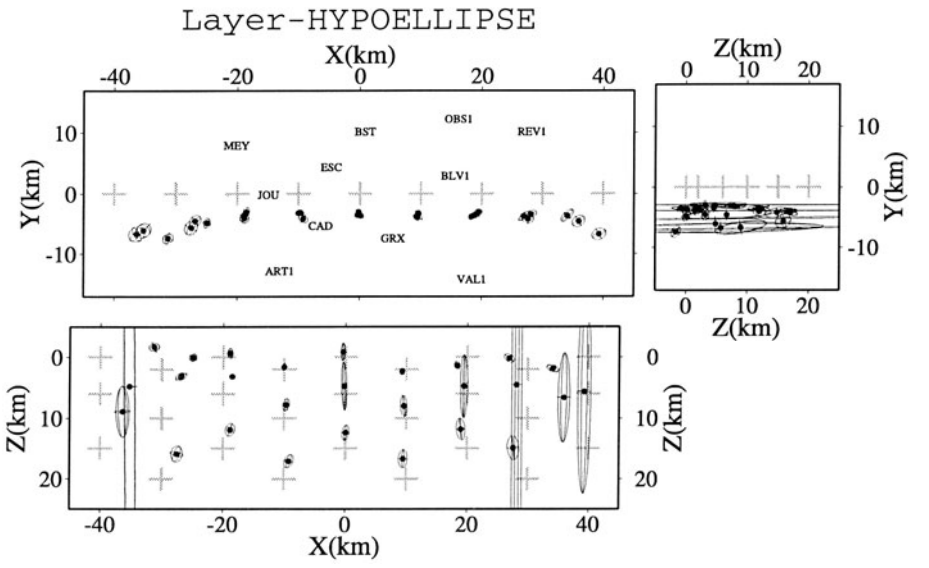

Figure 5. HYPOELLIPSE location with the layered model. Locations and 68% confidence ellipsoids in map view (XY), and views perpendicular (ZY) and parallel (XZ) to the event plane. Crosses: true event locations; stars: maximum likelihood hypocenters, dots: expectation hypocenters, ellipses: projections of 68% confidence ellipsoids.

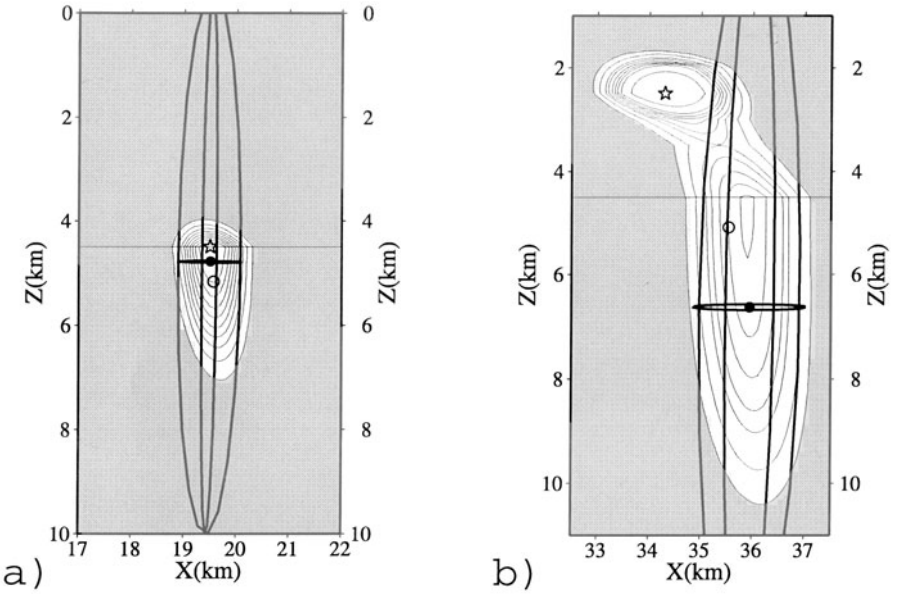

Figure 6. Grid-search and HYPOELLIPSE locations for (a) event [20,5] and (b) event [36,7]. Grid-search PDF: (white contoured region) - XZ slice of grid-search 90% confidence volume with a contour interval of 10%. Star: maximum likelihood hypocenter, open circle: expectation hypocenter. HYPOELLISE location - ellipses: projections of 68% confidence ellipsoid, large dot: expectation hypocenter.

system ill-conditioned and cause instability in the hypocenter depth perturbations; this may explain why the location of the hypocenter is not at a maximum of the PDF.

HYPOELLIPSE has convergence problems or produces a confidence ellipsoid that is a poor estimate of the complete PDF when the PDF is strongly non-ellipsoidal. This is expected since a local linearization gives a poor representation of the global properties of an irregular function. In effect, an irregular PDF implies a strongly non-linear problem.

5.4 Average station residuals and station "statics"

We next investigate the relation of average station residuals to the known static shifts in the arrival times. Figure 7 shows the applied 3D model static shifts, theoretical layered model static shifts, and average residuals for each phase at each station for different location scenarios. The theoretical layered model statics are given by the sum of the 3D model statics and the travel time difference between the 3D model times and the layered model times. For the goal of obtaining station adjustments to give improved absolute

event locations, the average station residuals should match the corresponding applied static shifts.

As expected, the average station residuals are effectively zero for locations using the exact synthetic travel times and the correct 3D model with both Metropolis-Gibbs (dots in Figure 7) and the grid-search (not shown).

The average station residuals for Metropolis-Gibbs locations in the correct 3D model using the synthetic travel times with station statics (stars in Figure 7) generally follow the true station statics in both polarity and amplitude. However, there are some significant mismatches (i.e. BST P and S, MEY P, VAL1 P) which can be attributed to the fact that the average station residuals are calculated for incorrect, though optimal, locations, and so reflect location errors as well as model errors. It may be expected that an iterative simultaneous inversion for true statics and event locations beginning with these average residuals will converge to near the correct solutions.

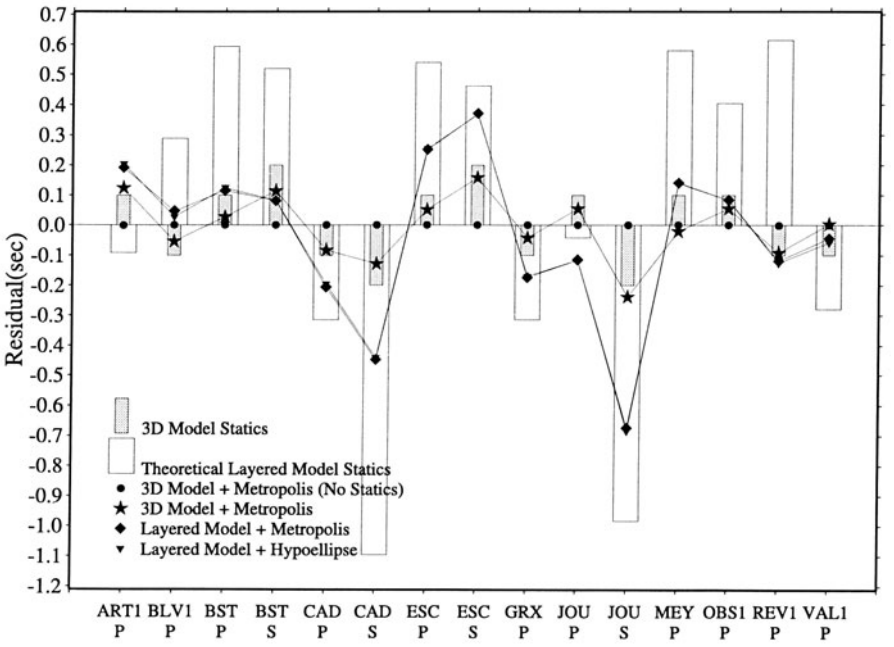

Figure 7. Comparison of station statics and average station residuals. (grey bars) True 3D model station statics (static shift in Table 1). (white bars) True layered model station statics (added static shift in Table 1 plus travel time difference between layered and 3D models for the "true" event location). Average station residuals (observed – calculated arrival times) for the maximum likelihood hypocenters are shown by symbols and lines for several location scenarios.

The average station residuals for the Metropolis-Gibbs and HYPOELLIPSE locations in the layered model (diamonds and triangles in Figure 7) are nearly identical. This agreement reflects the similarity in optimal hypocenters from both methods for most events. However, these residuals do not match and generally have much lower amplitude than the theoretical layered model statics. As above in the 3D case, this mismatch can be attributed to the fact that the average station residuals are calculated for incorrect locations, but with the layered model these locations are much further from the "true" locations. In this case it does not seem likely that a simultaneous inversion for true statics and event relocations beginning with these average residuals will necessarily converge towards the correct solutions. In general there is a better match between average residuals and theoretical statics for stations in the middle of the network (*i.e.* CAD, ESC, GRX and JOU) than for stations on the edge of the network (*i.e.* ART1, BST, OBS1, REV1 and VAL1). This pattern is consistent with the greater variety of paths and coverage of the model for rays between the internal stations and the events than for the external stations.

We have checked the sensitivity of this analysis to the particular set of static shifts used (Table 1) by repeating the locations using a reversed polarity for all of the static shifts. We found that all of the conclusions in this subsection were effectively unchanged.

5.5 Mechanisms

In this section we examine the quality of the recovery of known focal mechanisms in the various location scenarios. Synthetic P first-motions (up or down) corresponding to a pure left-lateral mechanism (strike=90°, dip=90°, rake=180°) were calculated along with the travel time for each synthetic arrival in the 3D velocity model. For each event location, the ray take-off angles are calculated at the optimal hypocenter (maximum likelihood point of PDF for the non-linear, global search methods, final hypocenter for HYPOELLIPSE). Using these synthetic first motions and location dependant take-off angles, composite focal mechanisms (Figure 8) are determined with the grid-search algorithm FPFIT (Reasenberg and Oppenheimer, 1985).

As is expected, the composite focal mechanism for the exact synthetic travel times and the correct 3D model (Figure 8a) is nearly identical to the synthetic left-lateral mechanism. The distribution of first-motion polarities on the focal sphere allows the exact synthetic mechanism as a possible solution with no discrepant observations out of 297 total. Figure 8b shows the composite focal mechanism for Metropolis-Gibbs locations in the 3D model using the synthetic travel times with station statics. For this case

there are now 10 discrepant observations, but the preferred focal mechanism remains very similar to the synthetic mechanism.

The composite focal mechanisms for Metropolis-Gibbs and HYPOELLIPSE locations in the layered model using the 3D model synthetic travel times with station statics are shown in Figures 8c and 8d. The Metropolis-Gibbs and HYPOELLIPSE results have, respectively, up to 6 and 10° errors in rake direction, and 43 and 48 discrepant observations. These differences from the synthetic mechanism are significant, but not extreme. This indicate that it is possible to have good recovery of a true composite solution using an incorrect velocity model, if a large and well distributed set of events is available and it can be assumed that they all have the same mechanism.

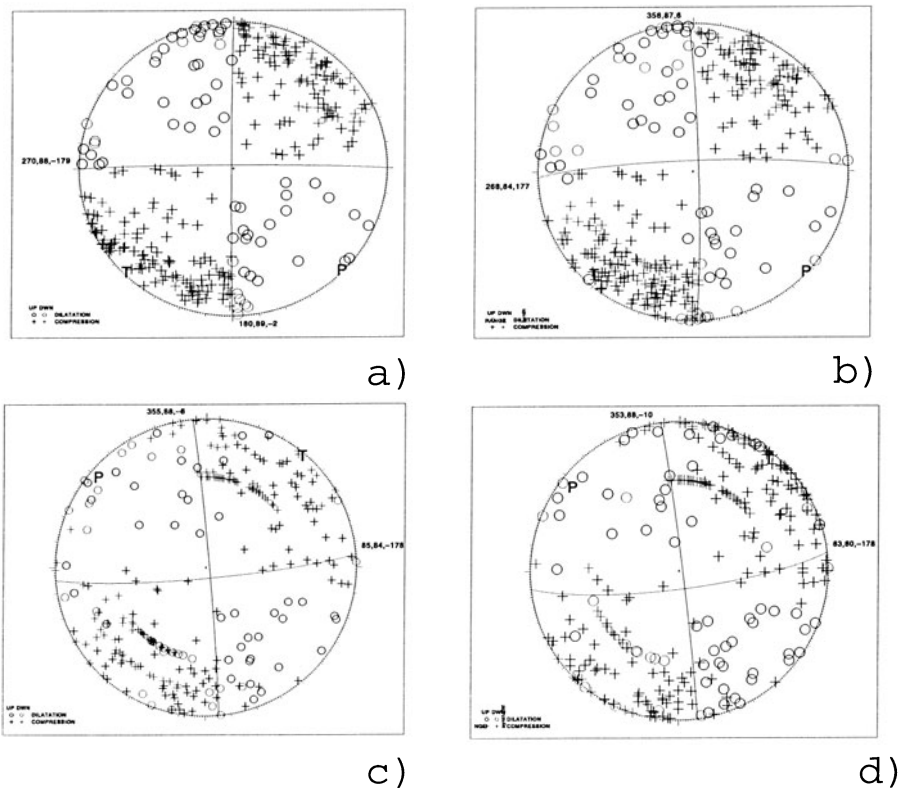

Figure 8. Composite focal mechanisms for Metropolis-Gibbs locations in the 3D model with (a) exact travel times and (b) station statics, and layered model locations using (c) Metropolis-Gibbs and (d) HYPOELLIPSE. Because of coordinate rotation, the positive Y axis of the location plots falls along the azimuth N30°E on these mechanism plots.

We do not investigate individual event mechanisms in detail because the number of observations and coverage of the focal sphere is not adequate to constrain well these solutions. Thus, for all location scenarios, including the exact, 3D case, the single preferred solution given by FPFIT differs significantly from the synthetic left-lateral mechanism for most events outside the network and for many events inside. However, for locations in the 3D model the distribution and polarity of first motions on the focal sphere remain compatible with the synthetic solution. That is, there are no discrepant data for the exact, 3D case and few discrepant data for the 3D case with station statics. This is not the case for the layered model locations where the ray take-off angles often have large errors due to strong velocity model errors and large absolute location errors.

6. DISCUSSION

We have described a complete, probabilistic earthquake location methodology and introduced an efficient Metropolis-Gibbs, non-linear, global sampling algorithm to obtain such locations. With several synthetic location scenarios, we have examined the locations and uncertainties given by an exhaustive grid-search and the Metropolis-Gibbs sampler using 3D and layered velocity models, and by the iterative, linearized method HYPOELLIPSE in the layered model.

With an exact 3D model and no added station static shifts, the grid-search and Metropolis-Gibbs location results are nearly identical and give excellent recovery of the true event location. However, because the location PDFs vary as a function of the event-station geometry, the location uncertainties can be large and irregular outside of the station network even for this exact case.

With an exact 3D model and added station static shifts there are systematic biases in the event locations. The PDFs and 68% confidence ellipsoids are similar in size and orientation to those for the case without statics, but for many events these error indicators do not include the "true" location.

The locations using the incorrect, layered model show that both linear and global methods give systematic biases in the event locations and that the 68% confidence volumes do not include the "true" location – absolute event locations and errors are not recovered. The results indicate that HYPOELLIPSE and related linearized, local methods can give stable and complete location and uncertainty results within a network, except for hypocenters near strong gradients in velocity. Outside a network these methods may have problems with depth determination, depth uncertainty

estimation, and even epicentral location. In contrast, the grid-search and Metropolis-Gibbs sampler global methods are always stable and give complete solution information, even near velocity gradients and outside of a network.

Our examination of average station residuals indicate that theoretical station statics can be recovered approximately if a model similar to the true velocity structure is available. However, if a poor model is used for location, then the average station residuals can be affected strongly by event location errors and will not be representative of the true station statics.

Our analysis of focal mechanisms shows that composite mechanisms can be recovered very well if a good velocity model is available, and fairly well even with a poor model. Individual event mechanisms, however, can be erroneous if there are few readings, or if a poor velocity model is used when there are strong lateral variations in the true structure.

HYPOELLIPSE and related linearized approaches are very fast and do not require significant computer memory. However, these methods are difficult or impossible to apply in 3D velocity structures, and they can fail if the location PDF is irregular or multi-modal. The systematic grid-search algorithm we use here is inefficient, about 1000 times slower than HYPOELLIPSE, but will generally give accurate recovery of the complete, probabilistic location PDF. However, if not selected carefully, the grid-search volume can clip parts of the location PDF; this problem can be avoided with an adaptive algorithm. Our implementation of the more efficient Metropolis-Gibbs sampler is only about 10 times slower than HYPOELLIPSE but may require considerable memory with 3D models. The Metropolis-Gibbs sampler gives good recovery of complete, probabilistic location PDFs, except for those that are highly irregular or multi-modal with widely separated maxima.

Thus the Metropolis-Gibbs sampler is a practical method to obtain complete, probabilistic locations for large numbers of events and for location in 3D models. With layered models, the Metropolis-Gibbs sampler is stable for cases where linearized methods fail, including locations near sharp contrasts in velocity and outside of a network. The grid-search method is useful for location of smaller number of events and to obtain an accurate images of location PDFs that may be highly-irregular.

ACKNOWLEDGEMENTS

We thank Pascal Podvin for providing the computer code for the calculation of finite differences travel times. This work was funded in part

by the Institut de Protection et de Sûreté Nucléaire and in part by the European Commission "TOMOVES" project ENV4 4980698.

REFERENCES

Aki, K., and P.G. Richards (1980) *Quantitative seismology*, W.H. Freeman, San Francisco.

Billings, S.D. (1994) Simulated annealing for earthquake location, *Geophys. J. Int.*, **118**, 680-692.

Calvert, A., F. Gomez, D. Seber, M. Barazangi, N. Jabour, A. Ibenbrahim, A. and Demnati (1997) An integrated geophysical investigation of recent seismicity in the Al-Hoceima region of North Morocco, *Bull. Seism. Soc. Am.* **87,** 637-651.

Dreger, D., R. Uhrhammer, M. Pasyanos, J. Frank, and B. Romanowicz (1998) Regional and far-regional earthquake locations and source parameters using sparse broadband networks: A test on the Ridgecrest sequence, *Bull. Seism. Soc. Am.* **88**, 1353-1362.

Geiger, L. (1912) Probability method for the determination of earthquake epicenters from the arrival time only (translated from German), *Bull. St. Louis Univ.* **8** (1), 56-71.

Goldberg, D.E. (1989) *Genetic Algorithms in Search, Optimization and Machine Learning*, Addison-Wesley, Reading, MA.

Goldberg, D.E., and J. Richardson (1987) Genetic algorithms with sharing for multimodal function optimization, in J.J. Grefenstette (Ed.), *Genetic Algorithms and their Applications, Proceedings of the Second International Conference on Genetic Algorithms and their applications*, Lawrence Erlbaum Associates, Hillsdale, NJ, 41-49.

Gresta, S., L. Peruzza, D. Slejko and G. Distefano (1998) Inferences on the main volcano-tectonic structures at Mt. Etna (Sicily) from a probabilistic seismological approach, *J. Seis.* **2**, 105-116.

Hammersley, J.M., and D.C. Handscomb (1967) *Monte Carlo Methods*, Methuen, London.

Holland, J.H. (1992) *Adaptation in natural and artificial systems*, Bradford Books/MIT Press, Cambridge, MA, 211 pp.

Jones, R.H., and R.C. Stewart (1997) A method for determining significant structures in a cloud of earthquakes, *J. Geophys. Res.* **102**, 8245-8254.

Keilis-Book, V.I., and T.B. Yanovskaya (1967) Inverse problems in seismology (structural review), *Geophys. J. R. Astr. Soc.* **13**, 223-234.

Kennett, B.L.N. (1992) Locating oceanic earthquakes – the influence of regional models and location criteria, *Geophys. J. Int.* **108**, 848-854.

Kirkpatrick, S., C.D. Gelatt, and M.P. Vecchi (1983) Optimization by simulated annealing, *Science* **220**, 671-680.

Lahr, J.C. (1989) HYPOELLIPSE/Version 2.0: A computer program for determining local earthquake hypocentral parameters, magnitude and first motion pattern, *U.S. Geol. Surv. Open-File Rep.* **89-116**, 92p.

Lepage, G.P. (1978) A new algorithm for adaptive multidimensional integration, *J. Comp. Phys.* **27**, 192-203.

Le Meur, H. (1994) Tomographie tridimensionelle a partor des temps des premieres arrivées des ondes P et S, application a la région de Patras (Grece), *These de Doctorate*, Université Paris VII, France.

Le Meur, H., J. Virieux, and P. Podvin (1997) Seismic tomogrphy of the Gulf of Corinth: a comparison of methods, *Ann. Geofis.* **40**, 1-24.

Lomax, A., and R. Snieder (1995) Identifying sets of acceptable solutions to non-linear, geophysical inverse problems which have complicated misfit functions, *Nonlinear Processes in Geophys.* **2**, 222-227.

Mohammadioun G., and P. Dervin (1995) A full scale laboratory for seismic studies in Southeastern France: The Middle Durance Fault, in *Proc. 5th International Conference on Seismic Zonation, Ouest Editions*, **2**, 1635-1642

Metropolis, N., A.W. Rosenbluth, M.N. Rosenbluth, A.H. Teller, and E. Teller (1953) Equation of state calculations by fast computing machines, *J. Chem. Phys.* **1**, 1087-1092.

Mosegaard, K., and A. Tarantola (1995) Monte Carlo sampling of solutions to inverse problems, *J. Geophys. Res.* **100**, 12431-12447.

Moser, T.J., T. van Eck, and G. Nolet (1992) Hypocenter determination in strongly heterogeneous earth models using the shortest path method, *J. Geophys. Res.* **97**, 6563-6572.

Nelson, G.D., and J.E. Vidale (1990) Earthquake locations by 3-D finite-difference travel times, *Bull. Seism. Soc. Am.* **80**, 395-410.

Nolte, B., and L.N. Frazer (1994) Vertical seismic profile inversion with genetic algorithms, *Geophys. J. Int.* **117**, 162-178.

Pavlis, G.L. (1986) Appraising earthquake hypocenter location errors: a complete practical approach for single event locations, *Bull. Seism. Soc. Am.* **76**, 1699-1717.

Podvin, P. and I. Lecomte (1991) Finite difference computations of traveltimes in very contrasted velocity models: a massively parallel approach and its associated tools, *Geophys. J. Int.* **105**, 271-284.

Press, F. (1968) Earth models obtained by Monte Carlo inversions, *J. Geophys. Res.* **73**, 5223-5234.

Press, W.H., S.A. Teukolosky, W.T. Vetterling, and B.P. Flannery (1993) *Numerical recipies in C: the art of scientific computing*, Cambridge Univ. Press, Cambridge, 994 pp.

Reasenberg, P. and D. Oppenheimer (1985) FPFIT, FPPLOT and FPPAGE: FORTRAN computer programs for calculating and plotting earthquake fault-plane solutions, *U.S. Geol. Surv. Open-File Rep.* **85-739**, 109p.

Rothman, D.H. (1985) Nonlinear inversion, statistical mechanics, and residual statics estimation, *Geophysics* **50**, 2784-2796.

Sambridge, M. and G. Drijkoningen (1992) Genetic algorithms in seismic waveform inversion, *Geophys. J. Int.* **109**, 323-342.

Sambridge, M. and K. Gallagher (1993) Earthquake hypocenter location using genetic algorithms, *Bull. Seism. Soc. Am.* **83** 1467-1491.

Sambridge, M.S., and B.L.N. Kennett (1986) A novel method of hypocenter location, *Geophys. J. R. Astron. Soc.* **87**, 313-331.

Scales, J. A., M. L. Smith, and T.L. Fischer (1992) Global optimization methods for multimodal inverse problems, *J. Comp. Phys.* **103**, 258-268.

Schwartz, S.Y., and G.D. Nelson (1991) Loma Prieta aftershock relocation with S-P traveltimes: effects of 3D structure and true error estimates, *Bull. Seism. Soc. Am.* **81**, 1705-1725.

Shearer, P.M. (1997) Improving local earthquake locations using the L1 norm and waveform cross correlation: Application to the Whittier Narrows, California, aftershock sequence., *J. Geophys. Res.* **102**, 8269-8283.

Sen, M.K., and P.L. Stoffa (1995) *Global optimization methods in geophysical inversion*, Elsevier, Amsterdam, 281p.

Stoffa, P.L., and M.K. Sen (1991) Nonlinear multiparameter optimization using genetic algorithms: Inversion of plane-wave seismograms, *Geophysics* **56**, 1794-1810.

Tarantola, A. (1987) *Inverse problem theory: Methods for data fitting and model parameter estimation*, Elsevier, Amsterdam, 613p.

Tarantola, A. and B. Valette (1982) Inverse problems = quest for information, *J. Geophys.*, **50**, 159-170.

Vidale, J.E. (1988) Finite-difference calculation of travel times, *Bull. Seism. Soc. Am.*, **78**, 2062-2078.

Vilardo, G., G. De Natale, G. Milano, and U. Coppa (1996) The seismicity of Mt. Vesuvius, *Tectonophys.*, **261**, 127-138.

Volant P., C. Berge, P. Dervin, M. Cushing., G. Mohammadiou and F. Mathieu (2000) The Southeastern Durance fault permanent network: preliminary results, *J. Seism.*, in press.

Wiggins, R. A. (1969) Monte Carlo inversion of body wave observations, *J. Geophys. Res.* **74**, 3171-3181.

Wittlinger, G., G. Herquel, and T. Nakache (1993) Earthquake location in strongly heterogeneous media, *Geophys. J. Int.* **115**, 759-777.